Published in final edited form as:
Annu Rev Phys Chem. 2010 ; 61: 345–367. doi:10.1146/annurev.physchem.012809.103444.

Superresolution Imaging using Single-Molecule Localization

George Patterson[1], **Michael Davidson**[2], **Suliana Manley**[3], and **Jennifer Lippincott-Schwartz**[4]

Jennifer Lippincott-Schwartz: lippincj@mail.nih.gov

[1]Biophotonics Section, National Institute of Biomedical Imaging and Bioengineering, National Institutes of Health, Bethesda, Maryland 20892

[2]National High Magnetic Field Laboratory and Department of Biological Science, The Florida State University, Tallahassee, Florida 32310

[3]École Polytechnique Fédérale de Lausanne, Lausanne, Switzerland CH-1015

[4]Cell Biology and Metabolism Program, Eunice Kennedy Shriver National Institute of Child Health and Human Development, National Institutes of Health, Bethesda, Maryland 20892

Abstract

Superresolution imaging is a rapidly emerging new field of microscopy that dramatically improves the spatial resolution of light microscopy by over an order of magnitude (~10–20-nm resolution), allowing biological processes to be described at the molecular scale. Here, we discuss a form of superresolution microscopy based on the controlled activation and sampling of sparse subsets of photoconvertible fluorescent molecules. In this single-molecule based imaging approach, a wide variety of probes have proved valuable, ranging from genetically encodable photoactivatable fluorescent proteins to photoswitchable cyanine dyes. These have been used in diverse applications of superresolution imaging: from three-dimensional, multicolor molecule localization to tracking of nanometric structures and molecules in living cells. Single-molecule-based superresolution imaging thus offers exciting possibilities for obtaining molecular-scale information on biological events occurring at variable timescales.

Keywords

superresolution microscopy; single molecule; PALM; STORM; FPALM; diffraction limit; photoactivation; photoactivatable fluorescent protein; fluorescence imaging

Introduction

Fluorescence microscopy, a favorite tool of biologists, magnifies and images light-emitting objects with a resolution down to one-quarter of a micrometer, enabling the study of fine structural details of cellular architecture and dynamics. Key insights into events occurring inside cells, tissues, and whole organisms have thereby been achieved, such as the shape of intracellular transport vehicles (1), the mechanism(s) for tissue remodeling (2), and the movement of cancer cells within a diseased organism (3). Contributing to the dramatic rise in fluorescence microscopy has been the advent of genetically encoded fluorescent proteins (FPs) acting as endogenous labels, allowing almost any protein or peptide to become fluorescent inside cells and thereby to be visible within a biological context (4). The wide

Disclosure Statement: The authors are not aware of any affiliations, memberships, funding, or financial holdings that might be perceived as affecting the objectivity of this review.

availability of sensitive cameras, inexpensive lasers, and high-quality optical lenses and filters has further permitted acquisition of superior images with spatiotemporal characteristics appropriate for addressing a diverse array of biological questions.

Despite its revolutionary impact, fluorescence microscopy faces a limit in its resolving capability—the diffraction of light. Arising from the wavelike character of light diffracting while passing through a lens, this limitation prevents objects smaller than ~250 nm along the *x*-*y* axis and ~500 nm in the *z* axis from being seen as anything but a blur. As many subcellular structures have features much smaller than this size—including microtubules, actin fibers, ribosomes, transport vesicles, and the intramembrane organization of organelles —the need to break the diffraction barrier, imaging below the size limitation it defines, has been the holy grail of light microscopy for many years (5).

Recently, two distinct conceptual strategies have overcome light's diffraction barrier, allowing the analysis of biological structures at the superresolution level. One strategy, referred to here as illumination-based superresolution, uses nonlinear optical approaches to reduce the focal spot size, as in stimulated emission depletion (STED) fluorescence microscopy (6) and saturated structured illumination microscopy (SSIM) (7). By modifying the excitation light pattern to yield a smaller spot size, STED and SSIM can resolve fine structural details of biological specimens, such as the shape of mitochondrial membranes (8) and chromosomal and nuclear envelope organization (9), down to ~30 nm in the *x*-*y* direction in the case of STED and ~100 nm in the case of SSIM.

The second strategy for overcoming light's diffraction barrier uses photoswitchable molecules to resolve dense populations of molecules with superresolution. This approach employs stochastic activation of fluorescence to switch on individual photoactivatable molecules and then images and bleaches them, temporally separating molecules that would otherwise be spatially indistinguishable. Merging all the single-molecule positions obtained by the photoactivation and imaging/bleaching cycles yields a final superresolution image. Referred to here as probe-based superresolution, this approach was independently developed by three groups and given the names photoactivated localization microscopy (PALM) (10), fluorescence photoactivated localization microscopy (FPALM) (11), and stochastic optical reconstruction microscopy (STORM) (12). Whereas PALM/FPALM use photoactivatable or photoconvertible FPs as probes, STORM uses synthetic fluorophores as probes, as in the photoswitchable fluorophore combination of Cy3 and Cy5. Probe-based superresolution allows biological structures to be defined with nanometric accuracy, similar to illumination-based superresolution. However, it additionally permits molecules comprising subcellular structures to be individually identified at high densities and their distributions and dynamics to be analyzed. This opens many new possibilities for addressing mechanistic questions regarding biological function, including the mapping of molecular machinery, its stoichiometry, and dynamics.

Both illumination-based and probe-based superresolution imaging approaches permit biologists to now visualize structures and processes of cells at or near the molecular level. The order-of-magnitude improvement in spatial resolution achieved over previous light microscopy methods means that the new approaches have enormous potential for addressing numerous biological questions requiring resolutions below 250 nm. So far, these approaches have provided details on the fine architecture of cell structures such as mitochondria, lysosomes, focal adhesions, microtubules, and coated vesicles (8, 10, 13). Dynamic processes have also been studied, including the movement of focal adhesion complexes (14) and bacteria polarity complexes (15), as well as single molecules on the plasma membrane (16, 17).

Here, we focus on probe-based superresolution imaging achieved using the single-molecule localization techniques of PALM/FPALM/STORM. We begin by discussing the concept underlying its development and the photoswitchable probes that it utilizes. We then describe its current state of development, including its various applications and limitations. We end by discussing the future possibilities and challenges of probe-based superresolution imaging, and the scientific areas it is likely to strongly impact.

Conceptual Basis of Probe-Based Superresolution Imaging

The principle of probe-based superresolution imaging rests on a combination of two capabilities: the imaging of single fluorophores and the controlled activation and sampling of sparse subsets in time of such fluorescent labels. Single-molecule imaging was initially demonstrated over a decade ago, first at cryogenic temperatures (18) and later at room temperature with near-field optics (19), and has since evolved to standard microscopy techniques. The prior knowledge that a diffraction-limited image of a molecule originates from a single source allows one to estimate the location (center) of that molecule with a precision well beyond the diffraction limit. This precision scales with the inverse square of the number of detected photons (20) (Figure 1a). Thus ~10-nm localization of that molecule can be established with ~1000 photons ina low background situation. Extension of this insight has resulted in many beautiful experiments studying isolated structures that are separated by $>0.3\ \mu m$ (i.e., the diffraction limit), such as labeled molecular motors (21, 22). The recent availability and ease of use of EMCCD (electron multiplying charge coupled device) cameras, with their single-photon sensitivity, have made this an easily implementable technique. The vast majority of proteins of interest in a biological system, however, are very densely distributed, with significantly more than one molecule sharing a diffraction-limited volume. In these cases, single-molecule-scale localization, as described above, is impossible because the fluorescence image of molecules formed appears as a highly overlapping distribution of fuzzy diffraction-limited spots. The way around this problem is to localize sparse subsets of molecules. That was first implied by an early experiment (23) in which individual densely distributed luminescent centers in a quantum well with distinct spectra were resolved by imaging with a sufficiently finely binned wavelength. Therefore, although there were many centers within a spatial resolution volume, they became resolvable when separated along another dimension, in this case, the wavelength. Within this higher-dimensional volume of x, y spatial coordinates and wavelength, it was possible to select a sufficiently sparse subset so that one could see the centers individually. This led to a generalization (24) that if the luminescence or fluorescence response from multiple sources could be spread out in some higher-dimensional space, then it could be possible to image the sources individually, localize each of their centers, and accumulate the center coordinates to create a superresolution image. Unfortunately this was not practical in the 1990s with the fluorescent labels available for biological systems as labels with the requisite attributes (e.g., separable narrow wavelengths) were not known.

This changed with the discovery of photoactivatable fluorescent labels (25, 26) when it became possible to switch on thousands of sparse subsets of molecules created sequentially in time (10). The operating principle of this method is to start with the vast majority of labels in an inactive state, not contributing to the fluorescence. A small fraction ($\ll$1 part in 100) is then activated and made capable of fluorescence. This activation can be achieved by illumination with near-ultraviolet (near-UV) light that causes a chemical modification in a few molecules and allows fluorescence. That sparse subset is then imaged, and each fluorescent label can then be localized to give nanometer-level precision coordinates. Those labels are then removed (e.g., by bleaching) so that a new sparse subset can be put into the active state and sampled to add a new set of molecular coordinates (Figure 1b). This process

can be repeated many thousands of times so that up to millions of such molecular coordinates can be accumulated within an imaged area. By rendering a composite image of all these coordinates, a single-molecule superresolution image of the labeled protein or structure is thereby created (Figure 1c). The molecular coordinates are not represented by only a point, showing their *x*, *y* location, but by a Gaussian intensity corresponding to the positional uncertainty of their location. Care must be taken to count each molecule only once even if its fluorescence is blinking.

Probes for Single-Molecule Superresolution Microscopy

Several fluorophore classes have emerged as candidates for labeling subcellular targets in photoactivated localization single-molecule microscopy. These include genetically encoded FP fusions, small-molecule synthetic dyes, quantum dots, and hybrid systems that combine a genetically encoded target peptide with a separate synthetic component that is membrane permeant. Each class of probes has its particular strengths and weaknesses, but no single class or individual fluorophore has been developed that combines all the preferred characteristics of an ideal probe for single-molecule superresolution microscopy (27–29). The principal criterion for fluorescent probes in this class is that they must be capable of being photoactivated, photoswitched, or photoconverted by light of a specific wavelength as a means to alter their spectral properties for the detection of selected subpopulations.

Among the most desirable attributes for single-molecule superresolution probes are very high brightness and contrast levels, which are necessary to maximize the number of photons that can be detected per molecule before it photobleaches or reverts to a dark state. Brightness is determined by the product of the molar extinction coefficient (ε_{abs}) and the fluorescence quantum yield (φ) (30). Thus, the best probes have high extinction coefficients and quantum yields and provide excellent contrast over the background (10, 27). In addition, photoswitching properties should include spectral profiles for the active and inactive species that are sufficiently well separated and thermally stable so that spontaneous interconversion energies are very low compared with the light-controlled activation energy. Ideally, these probes should also exhibit high switching reliability, low fatigue rates (the number of survivable switching cycles), and switching kinetics that can be controlled (28). In terms of photobleaching or photoswitching to a dark state, the best probes are those whose inactivation can be balanced with the activation rate to ensure that only a small population of molecules is activated (i.e., fluorescent) for readout, and that these activated molecules are separated by a distance greater than the resolution limits of the camera system. Furthermore, each photoactivated molecule should emit enough photons while in an activated state to accurately determine their lateral position coordinates (10, 31).

Aside from displaying the necessary fluorescent properties, single-molecule superresolution probes must also localize to their intended targets with high precision and exhibit the lowest possible background noise levels. Fluorescent proteins, hybrid systems, and highly specific synthetic fluorophores are able to selectively target protein assemblies or organelles, but most of the cadre of synthetics and quantum dots must first be conjugated to a carrier molecule for precise labeling. In many cases, the exact proximity of the probe to the target is questionable, as is the number of actual fluorophore units involved, especially when small synthetic dye molecules or quantum dots are conjugated to large antibodies (31). Additionally, variations in photophysical properties (such as fluorescence quantum yield) induced by environmental fluctuations or intermolecular interactions can complicate data analysis. Finally, regardless of whether localization analysis is performed on fixed or living cells, autofluorescence arising from fixatives and transfection reagents can often produce excessively high background signal (32).

Fluorescent Protein Probes

The intrinsic ability of certain FPs to alter their spectral properties upon exposure to light of a specific wavelength coupled with their excellent targeting specificity has been widely exploited in superresolution imaging (see Table 1). Although FPs are known to undergo a variety of light-induced switching characteristics, including distinct emission and nonemission states as well as on-and-off blinking behavior (33, 34), the most useful properties are photoactivation, photoconversion, and photoswitching, functions that can be collectively termed optical highlighting (35). Photoactivatable FPs are capable of being activated from a dark state to bright fluorescence emission upon illumination with UV or violet light, whereas photoconvertible FPs can be optically transformed from one fluorescence emission bandwidth to another. In contrast, photoswitchable FPs have emission characteristics that can alternatively be turned on or off with specific illumination. Aside from the requirement that FPs must display some type of optical highlighting behavior for superresolution imaging, they must also have sufficient brightness, chromophore maturation rates, and monomeric character to express the fusion without artifacts, such as mistargeting and dysfunction (27). Additionally, oligomerization in FPs can present a problem in stochastic superresolution microscopy as there is more than one chromophore in each localized probe molecule.

Photoactivatable fluorescent proteins—The first useful optical highlighter was engineered by substituting histidine for threonine at position 203in wild-type GFP to produce a photoactivatable version (termed PA-GFP) with negligible absorbance in the region between 450 and 500 nm (25). Upon photoactivation with violet or UV light, the absorption maximum of PA-GFP is shifted from 400 nm to 504 nm, accompanied by a 100-fold increase in fluorescence when excited at 488 nm. A complementary probe derived from coral is a photoactivatable variant of mCherry (named PA-mCherry1) having excitation and emission spectra at 564 and 595 nm, respectively (36). Compared with earlier red variants, the mCherry version features faster maturation, better pH stability, faster photoactivation, improved photostability, and higher contrast. As a highlighter, PA-mCherry1 has been demonstrated to be an excellent complement to PA-GFP for dual-color superresolution microscopy investigations.

Several additional photoactivatable FPs have been reported and may find utility in superresolution experiments. PS-CFP (photoswitchable cyan fluorescent protein) exhibits a significant level of cyan fluorescence prior to photoactivation with UV or violet light (37). Unfortunately, the fluorescence emission intensity of this probe is approximately twofold less than PA-GFP, significantly reducing the contrast ratio. Another probe, termed Phamret, couples PA-GFP to a high-performance ECFP variant through a two–amino acid linker to form a photoactivatable tandem dimer (38). When excited with 458-nm light, Phamret emits cyan fluorescence. The PA-GFP portion of Phamret can be photoactivated with 405-nm illumination to evoke Foörster resonance energy transfer between the ECFP and activated PA-GFP. After photoactivation, Phamret exhibits green fluorescence (520-nm peak) upon illumination at 458 nm and can therefore potentially be used as a localization probe. The major downside of Phamret is that two FP units were used to construct the highlighter, increasing the size and possibly creating steric hindrance in some fusions.

Photoconvertible fluorescent proteins—One of the most useful classes of optical highlighter probes for superresolution microscopy comprises the growing number of FPs reported to undergo photoconversion from one emission wavelength to another (principally, from green to red) (32, 35). Although a number of highly efficient FPs in this class have been reported, many are tetrameric in nature and thus are not useful as fusion markers. The first photoconvertible FP used in PALM imaging was obtained from a stony coral and

named EosFP (10, 39). This variant emits bright green fluorescence at 516 nm and can be photoconverted to orange-red (581 nm) fluorescence when illuminated at near-UV wavelengths. Random and site-directed mutagenesis of tetrameric EosFP was used to generate two dimers and a true monomeric protein named mEosFP (40). Unfortunately, the monomeric variant of EosFP can only be expressed efficiently at temperatures below 30°C, limiting the utility of mEosFP in mammalian systems. To create a pseudomonomer suitable for imaging fusions at 37°C, investigators linked two of the dimeric EosFP units together using a 16–amino acid linker to produce a tandem dimer (40). tdEosFP has turned out to be one of the most useful optical highlighters developed for superresolution imaging because of its high brightness levels and functionality as a tag in fusion vectors. Recently, an improved monomeric version that matures at 37°C, named mEos2, has been reported (30). Although not as bright as tdEos, mEos2 is an excellent complement for imaging problematic fusions (tubulin, histones, gap junctions) that localize poorly with tandem dimers.

Several other optical highlighters with green-to-red photoconversion properties are candidates for superresolution imaging, but these have not been adequately tested for performance. A tetrameric highlighter isolated from coral and named KikGR was subjected to extensive mutagenesis to yield a monomeric derivative containing 21 mutations (mKikGR) (41). Both the green and red forms of mKikGR are less photostable and feature less photon output than mEos2; however, this highlighter might perform better in tubulin and gap junction fusions (30). A monomeric variant of the tetrameric DendFP has been developed through random and site-directed mutagenesis and named Dendra (42). This highlighter features excitation and emission maxima for the green and red forms of 490/553 nm and 507/573 nm, respectively, and functions well in fusion tags for subcellular localization. The commercial version, Dendra2 (Evrogen), is the first monomeric red-to-green optical highlighter that has enjoyed widespread use as a tracking tool in live-cell imaging and may find utility in superresolution imaging.

A new and unique optical highlighter derived from wtEosFP couples the properties of photoconversion and photoswitching into a single reporter (43). Named IrisFP, a single mutation in wtEosFP (F173S) bestows reversible photoswitching (see below) induced by *cis-trans* isomerization of the chromophore in both the native (green) and photoconverted (red) species. Similar to the wild-type parent, IrisFP undergoes photoconversion from a green- to a red-emitting state upon illumination with violet (405 nm) or UV light. Illumination of the green IrisFP species with 488-nm laser light drives the highlighter to a nonfluorescent dark state, which can then revert to a bright species upon illumination with low-intensity 405-nm light. High-intensity 405-nm illumination drives the IrisFP chromophore to the red state. Similar to the green state of IrisFP, the red state can be photoswitched off with 532-nm light and back on again with 440-nm light. Although hampered for use in fusions by the tetrameric quaternary structure, IrisFP represents a new class of optical highlighters that will perhaps be exploited for superresolution microscopy in the future.

As a significant side note, it appears that photoconversion in FPs is far more widespread than originally suspected, as evidenced by observations of alterations to the emission spectral profiles of cyan and yellow FPs following photobleaching experiments. In a recent investigation (44), several of the orange and red Anthozoa proteins, including mOrange, mKate, and HcRed1, were observed to shift emission to longer or shorter wavelengths upon intense illumination using single- and two-photon laser sources, although the contrast ratios between the native and photoconverted species are low. Thus, it is possible that photoconversion is far more widespread than originally suspected, but harnessing the phenomenon into a useful tool for superresolution microscopy could still prove challenging.

Photoswitchable fluorescent proteins—Several optical highlighters have been isolated that can be reliably toggled on or off by illumination with different excitation wavelengths, and these are called photoswitchable FPs. The most prominent and well-studied member of this class is Dronpa (35, 45, 46), which is a monomeric variant derived from a stony coral tetramer. Dronpa exhibits an absorption maximum at 503 nm (arising from the anionic, deprotonated chromophore) with a minor peak at 390 nm (from the neutral, protonated chromophore). The anionic chromophore emits green fluorescence with a maximum at 518 nm and has a brightness level almost 2.5 times that of EGFP. Dronpa photoswitching occurs in part by interconversion between the deprotonated (on state; bright) and protonated (off state; dark) forms. Illumination at 488 nm drives Dronpa to the dark species, after which the FP can be subsequently switched back on by brief illumination at 405 nm. This cycle can be repeated several hundred times without significant photobleaching. The primary mechanism of FP photoswitching is thought to also arise from *cis-trans* isomerization of the hydroxybenzilidine (tyrosyl side chain) chromophore moiety that accompanies the changes in the protonation state, which may be an underlying mechanism that is common to all photoactivatable and reversibly photoswitchable FP derivatives. Similar to other highlighters, Dronpa is useful in superresolution studies (31), and variants of Dronpa with reversed photoswitching properties and broader spectra have been reported as candidates for superresolution imaging (47, 48). Future versions will no doubt feature higher brightness and should prove useful in dynamics investigations.

Several photoswitching FPs in other regions of the color palette have been developed from anemones and corals. Kindling FP (commercially available from Evrogen as KFP1) is a tetrameric highlighter that emits red fluorescence at 600 nm upon illumination with green or yellow light (525–580 nm) (49). Upon cessation of illumination, KFP1 relaxes back to its initial nonfluorescent state. Irradiation with intense blue light (450–490 nm) completely quenches KFP1 fluorescence immediately, enabling control over the photoswitching for superresolution imaging. A cyan FP from coral named mTFP0.7 (an intermediate in mTFP1 mutagenesis) has also been demonstrated to photoswitch (50), but has not been characterized. Inaddition, monomeric photoswitchable variants of mCherry have recently been introduced aspotential probes for superresolution microscopy (51). Termed rsCherry and rsCherryRev, these derivatives display antagonistic switching modes. Here, irradiation of rsCherry with yellow light induces the bright state, and blue light drives the FP to the dark state, whereas the reverse is observed with rsCherryRev. Unfortunately, these FPs are only ~10% as bright as mCherry when expressed as ensembles in cells, but are equally bright as mCherry on the single-molecule level.

Synthetic Fluorophores and Quantum Dots

Among the synthetic organic fluorophores and inorganic quantum dots that have the potential to be useful probes for superresolution imaging are several candidates that display reversible photo-switching and irreversible photoactivation (the latter are also referred to as caged fluorophores) (52). Unfortunately, there have been no reports to date of organic compounds or quantum dots that are capable of being photoconverted from one emission wavelength to another. The main advantage of using synthetic fluorophores and quantum dots is their high brightness, excellent photostability, good contrast, and greater fatigue resistance when compared to FPs (27). For example, tdEos yields approximately 500 photons per molecule in contrast to the 6000 photons observed for the photoswitchable fluorophore combination of Cy3 and Cy5. Furthermore, the cyanine dyes can undergo over 200 switching cycles before photobleaching (53). The primary disadvantage of using quantum dots and synthetic fluorophores is the difficulty in targeting specific locations and higher background signal when compared to FPs. The most reliable targeting scheme for fluorophores in this class is conjugation to a primary or secondary antibody, although

several new synthetic dyes have been demonstrated to localize in specific regions independently. Antibodies cannot permeate membranes and are therefore only useful in fixed and permeabilized cells unless the target is displayed on the outer region of the plasma membrane. Labeling with antibodies is also relatively low in efficiency and adds 10 to 20 nm to the localization uncertainty between the label and the target. In addition, conjugates of quantum dots to antibodies do not perform on par with analogous conjugates using synthetic dyes such as Alexa Fluors and cyanines.

Quantum dots are inorganic semiconductor nanocrystals composed of a CdSe core surrounded by a ZnS shell that exhibit fluorescent properties owing to confined exciton emission (54). A passivation layer and hydrophilic coating must be applied to quantum dots for biological applications, and they must also be conjugated to streptavidin or antibodies for targeting. The fluorescence emission profile of quantum dots is remarkably symmetrical and generally exhibits a large quantum yield, whereas their broad absorption profile enables them to be excited over a large wavelength range. The size of the CdSe core dictates the emission spectral profile, with smaller cores (~2 nm) emitting in the blue regions and larger cores (5–7 nm) emitting in the yellow and red wavelengths. In general, the photostability for quantum dots dramatically exceeds that of all other known fluorophores, including synthetic fluorophores and FPs, which creates a problem for stochastic superresolution imaging unless quantum dots can be converted into a photoswitchable state. Recently, investigators (55) demonstrated that manganese doping of ZnSe quantum dots can be used to generate a species that can be reversibly photoswitched with high efficiency using light without the requirement for external activators or quenchers (effectors). Targeting remains a problem with quantum dots; however, continued advancements in quantum dot chemistry will undoubtedly lead to new and better probes in this class.

Among the synthetic reversibly photoswitchable probes that have found utility in superresolution imaging are rhodamine derivatives, cyanine dyes (Cy2–Cy7), and Alexa Fluors (29, 53, 56). Several photochromic rhodamine derivatives have been demonstrated to photoswitch via a light-induced isomerization in the absence of effector molecules, but the cyanine and Alexa Fluor dyes require the assistance of a second fluorophore. In switching rhodamine B, the closed isomer can transiently form a brightly fluorescent species upon irradiation with UV or red light (57). Within a few milliseconds to minutes, depending upon the solvent environment, the reaction is thermally reversed. Imaging of the photoswitched species with 530-nm light excites fluorescence emission, but does not return the switched molecule to the native state. This is a desirable characteristic as the fluorescence emission can be monitored without erasing the fluorescent species, which results in a higher photon count per switching event. Improved synthetic photoswitchers, including new rhodamine derivatives and diarylethenes, should increase the utility of these probes in superresolution imaging provided that difficulties with water solubility and conjugation to antibodies can be overcome.

The photoswitchable cyanine dyes have been the most extensively used synthetic organicprobes in stochastic superresolution imaging (13, 29, 58). The near-infrared dye Cy5 has seen the most duty and can be used without an effector, although combining Cy5 with a secondary chromophore (such as Cy3, Cy2, or Alexa Fluor 405) dramatically facilitates photoswitching. As an example application, thecombinationofCy5 with Cy3 enables the use of a red laser (635 nm) to photoswitch Cy5 to a stable dark state, whereas exposure to 543-nm light converts Cy5 back to the fluorescent species. The rate of conversion back to the fluorescent species depends on the proximity of the secondary effector (Cy3). Additional combinations of cyanine and Alexa Fluor dyes, such as Cy3 and Cy5.5 or Cy7 and Alexa Fluor 647 with Cy2 or Cy3, have been reported, greatly expanding the available color palette for superresolution imaging (27, 29). Furthermore, a large number of commercially

available synthetics, including most of the Alexa Fluor and ATTO dye families (59), have been demonstrated to reversibly photoswitch infixed cells using a protocol that includes thiol-containing reducing agents (b-mercaptoethylamine, dithiothreitol, or glutathione) to generate a stable nonfluorescent state (28, 60). Thus, even though the switching mechanism has yet to be determined, the potential for generating synthetic organic photoswitchers for multicolor imaging currently surpasses the limited palette of FPs that undergo light-induced modulation.

Similar to the photoactivatable FPs (PA-GFP and PA-mCherry), a large library of caged synthetics would be especially useful for stochastic superresolution imaging. Unfortunately, only a few promising candidates have been reported to date: caged versions of fluorescein and rhodamine, which have been demonstrated to act in a manner similar to PA-GFP in PALM imaging. In practice, the caged synthetics are liberated from their protective ester groups using irradiation with UV light to generate a fluorescent species exhibiting excellent contrast that can be localized with high precision and then photobleached. Until a larger variety of caged fluorophores emerges, this class will remain limited in superresolution imaging applications.

The future of superresolution imaging relies on increasing the specificity and labeling efficiency of very bright photoswitchable fluorophores while simultaneously decreasing the size of the targeting peptides. A wide spectrum of hybrid systems designed to couple synthetic fluorophores with genetically encoded targets may one day be capable of achieving this goal (61, 62). All these systems utilize a peptide or protein sequence that is expressed in living cells and is capable of recruiting a small synthetic molecule to bestow fluorescence. The most developed candidate in this class utilizes a tetracysteine motif fused to a variety of genetic targets to recruit blue, green, or red fluorophores (FlAsH, ReAsH, or CHoAsH, respectively) capable of binding to the cysteine residues to generate a probe similar in specificity to FPs (63). The major disadvantage of these combinations is the inability to overcome the high background levels of unbound fluorophore that lower contrast. A number of other candidates have been developed, but none has seen significant use in superresolution imaging.

Survey of Molecular Localization Techniques

Numerous molecular localization techniques have been published that identify more than one molecule per diffraction-limited spot. As mentioned above, one of the first successful experiments in this field was accomplished on individual densely distributed luminescent centers in a quantum well. These were resolved by imaging with a sufficiently finely binned wavelength to separate the components (23). Spectrally selective imaging was used for pentacene molecules embedded in a *p*-terphenyl crystal and localized seven molecules located within the same spot at ~40-nm and ~100-nm precisions in the lateral and axial directions, respectively. The molecules were imaged individually by tuning the laser excitation to match the absorption of each molecule (64, 65). Heilemann et al. (66) took advantage of the different fluorescent lifetimes of the cyanine dye Cy5 and the rhodamine derivative JF9 to localize two different molecules fluorescing with similar wavelengths within the same diffraction-limited spot. Nanometer-localized multiple single-molecule fluorescence microscopy imaged fields of molecules until all were photobleached and utilized the different rates of photobleaching to localize the molecules in sequential intervals. The centroid determination started with the most photostable, marked its position, subtracted its fluorescence distribution from the next most photostable molecule, localized that molecule, and repeated the process. Through this process, up to five molecules were localized to <10-nm precision in the same spot (67). Lidke et al. (68) used blinking behavior to detect and localize two quantum dots within a diffraction-limited spot.

Whereas the techniques just described represent advances inprecisely localizing more than one molecule, PALM (10) and F-PALM (11) extended them to thousands of molecules using photoactivatable FPs. Concurrently, STORM was developed based on the photoswitching phenomenon of several cyanine dyes when located in close proximity (<2 nm) to each other (53). This allowed investigators to turn molecules on and off repeatedly in a controlled manner and thus maintain the required low density of detected molecules (12). Because these techniques advanced molecular localization to much higher numbers of molecules, this approach became relevant to cell biology studies and has led to many other developments based on similar principles.

Depending on the fluorophore, the molecules are synthesized as a dark molecule or they can be switched off. They become fluorescent again either by activation of a small pool or by stochastic return from a metastable dark state. For instance,PALMIRA(PALM with independently running acquisition) (69) uses photoswitchable FPs, but as with other techniques [dSTORM (direct STORM) (70), RPM (reversible photobleaching microscopy) (71), GSDIM (ground-state depletion microscopy with individual molecule return) (72), DH-PSF (double-helix point spread function) (73), and TL-PALM (time-lapse PALM) (15)], it uses photoswitching into dark states of several conventional fluorescent dyes, such as Cy5, Alexa 647, Alexa488, Texas Red, FITC, Rhodamine110, Oregon Green, Atto532, and Atto565. In addition, the conventional FPs [EGFP, EYFP (15), Citrine, and PhiYFP] have also been found to function in a similar manner (72), and several red and orange proteins undergo photoconversion (44). An initial irradiation step is required, often to produce the necessary low background for single-molecule imaging. This likely occurs through two possible mechanisms: photobleaching to single-molecule density and/or driving the population into metastable dark states.

Static high-density molecular localization—Given the relatively long time required to collect an image as compared with diffraction-limited wide-field or confocal imaging, static experiments represent the bulk of experiments in this field. Because the cells are usually fixed with an aldehyde derivative and are unlikely to undergo any structural alterations, the image acquisition time is not a critical factor and is normally dictated by the number of molecules in the sample and the patience of the investigator. These have led to images revealing the molecular organization of proteins within structures at nanometer resolution, and among the favorite structures to image have been the actin and microtubule networks. As they are distinct, well-characterized, <25-nm filaments located at various distances from each other, they make excellent resolution tests. Others include vinculin at focal adhesion sites and proteins embedded within the plasma membrane (10, 16, 31). Another prominent example is the sensory clusters comprising the *Escherichia coli* chemotaxis network (74), which were mapped at 15-nm resolution to show that cluster formation occurred via stochastic self-assembly without cytoskeletal involvement or active transport of components.

An interesting feature associated with single-molecule localization techniques is that the investigator can define which molecules are displayed. For instance, the investigator may decide to display only molecules that localize with better than 10-nm uncertainty. Here, molecular precision and the resolution obtainable with single-molecule localization must be distinguished. Although the location of molecules within a specimen can be determined to 1–2 nm in some cases, the stated resolution of distinct structural elements must obey the Nyquist criterion of sampling at approximately two data points per resolution unit. Thus, the density of the localized molecules becomes important for resolution claims. For example, Figure 2 shows a cow, Bossy, when her image is made up of an increasing number of points. At the lower densities, it is difficult to even determine that it is an image of any cow, much less an image of Bossy. As the density of the points increases, it becomes evident that the

image contains a cow's face, but it requires even more points to recognize Bossy. Single-molecule localization experiments face a similar problem. Images can be rendered with the molecules localized with the highest precisions, but this comes at the expense of the molecular density of the final image, which directly affects the resolution of the image.

Investigators may be faced with a similar problem simply based on the specimen and molecule of interest rather than an arbitrarily imposed limitation on molecular precision. This can occur from a normal low density of molecules within the specimen. For example, considering the size of a photoactivated FP with a diameter of ~2.5 nm, a two-dimensional plane, such as an organelle membrane, will have a maximum density of $\sim 2 \times 10^5$ molecules μm^{-2}. To reach such a high density, this assumes that only photoactivated FP tagged molecules are located in this plane. Molecules located in polymers may approach this level, but it is an unlikely physiological situation elsewhere in the cell. However, if photoactivated-FP-tagged proteins comprise 1% of the molecules in an organelle membrane, this leads to ~2000 molecules μm^{-2} (~2 molecules per 40–50 nm), which is a sampling density that pales in comparison to the obtainable molecular precision seen by electron microscopy and limits any resolution claims about structural features.

Nevertheless, experiments observing 2000 molecules μm^{-2} in an organelle membrane offer much information, despite any limits on resolution. They can reveal relative molecular distributions within the specimen, which is often the goal of an imaging experiment. However, this requires placing the data in the context of the rest of the specimen. Two approaches have been used so far to accomplish this: overlaying localized molecules with an electron micrograph of the same specimen (10) and, as discussed below, overlaying images of two different proteins localized in the same specimen via multicolor single-molecule localization.

Multicolor high-density molecular localization—Several strategies have been used to perform probe-based superresolution imaging using dual-color probes (31, 36, 75). The PALMIRA two-color scheme (75) employed photoswitchable rsFastlime paired with Cy5. The Dronpa derivative rsFastlime is switched on and off, whereas Cy5 is transitioned into a dark state from which it spontaneously reverts into a fluorescent molecule. Switching of the molecules into the dark state was utilized to maintain the low density of fluorescent molecules necessary for single-molecule imaging. STORM experiments utilized the controlled photoswitching behavior of multiple cyanine dye pairings tagged to antibodies to render two-color images of clathrin-coated pits and microtubules (13).

Equivalent experiments using two different colors of photoactivated FPs were hampered by either spectral overlap of the bright red photoconvertible FPs, such as EosFP, or low photon yield in red markers. However, in PALM experiments, Shroff et al. (31) were able to image the Dronpa/EosFP pairing by photoactivating and imaging EosFP until all were detected, localized, and photobleached before deactivating the Dronpa molecules using intense 488-nm light. These were reactivated, localized, and combined with the EosFP images to construct the final double-label image.

A more straightforward approach for two-color PALM experiments employed a green marker and a bright red molecule that has no spectral overlap with the green partner. This was made possible with the development of a photoactivatable version of the popular mCherry called PAmCherry1 (36). In these examples, the green partner, PA-GFP, and PAmCherry1 were both switched on with 405-nm light while a 488-nm and 561-nm light imaged PAGFP and PAmCherry1, respectively. Importantly, PAmCherry1 can also be used with several of the other green photoactivated FPs, such as Dronpa, rsFastlime, and PS-CFP2, and can perhaps lead to better precision.

Three-dimensional high-density molecular localization—Above we describe probe-based su perresolution imaging largely as a two-dimensional imaging technique. The third dimension is constrained by the sample thickness to ~100 nm if it is a microtomed section. Alternatively, a similar thickness of a sample adjacent to the glass surface can be probed with total internal reflection fluorescence excitation radiation. Additional vertical (*z*-axis) positional information can be revealed by a variety of techniques combined with photoactivation and localization. These fall into a few different categories: those that exploit a *z*-dependent point spread function, those that use a side-view approach, and those that harness interferometry along the axial direction.

The simplest example of a *z*-dependent point spread function is the defocusing of a point object that is above or below the ideal in-focus object plane. An image of such a point source can broaden, develop rings around a central peak, or otherwise evolve. One approach can capture two simultaneous images set to two slightly different object planes, i.e., one underfocused and one overfocused. A beam splitter followed by imaging detection set to two different imaging focal distances can accomplish this. The ratio of spot sizes is a monotonic function of axial position and can be parameterized. This biplane method (76) has achieved close to the standard PALM lateral resolution (degraded by only 20%–30%) and an axial resolution (degraded by another factor of ~2), giving ~75-nm full width at half-maximum with FPs. Its advantage is its relative simplicity in accessing the extra dimension. A similar over- and underfocus can be implemented along two orthogonal axes of one image, so that the *x* axis can focus at a different *z* position than the *y* axis (77). The addition of a weak cylindrical lens after the objective can produce this effect. In this way, a point source produces an elliptical image, with the ratio of *x* and *y* diameters reflecting a monotonic function of its axial position. Readout of fluorescent ellipticities has given similar lateral and 50–60-nm vertical resolution for a given number of detected photons for Cy3-Cy5 dye pairs. More exotic *z*-dependent point spread functions have been produced with a spatial phase modulator. In particular, a double point image can be generated from a single source, but then the angular orientation of this doublet is dependent on the *z* axial position (73). The angular orientation can be used as a readout of the axial position. As an alternative to spatial focusing, femtosecond pulses of excitation light can be focused in time (78). This requires a more sophisticated setup and is dependent on two-photon excitation rather than linear single-photon approaches. However, it has an interesting advantage of reducing spurious excitation or activation in planes outside the thickness of interest. This preserves photoactivatable fluorescence, enabling multiple 1.0-μm-thick planes to form stacks of PALM images up to 10 μm thick.

The best resolution can be achieved with interferometry combined with PALM.This technique, called iPALM, has demonstrated 10-nm vertical and 20-nm lateral full width at half-maximum localization of FP labels (79). Interferometry is a common position measurement technique that is based on how light interferes after it has taken two different position-dependent paths and is then combined with a beam splitter. The special requirements of coherence, calibration, and tolerance of the highly unstable fluctuating nature of fluorescence dictate the implementation. Coherence can be maintained by realizing that any emitted photon is always coherent against itself. Interfering the same photon that takes two paths with different *z*-dependent path lengths satisfies this first requirement. The self-calibration requirement is also fulfilled by single-photon self-interference and can be tolerant to fluctuations of a fluorescent source by using simultaneous multiphase interferometry. To implement this over a unique wide field, investigators developed a multiphase beam splitter that has been successfully demonstrated on resolving membranes, microtubules, endoplasmic reticulum, and focal adhesion architecture (79) (Figure 3). While achieving the best spatial localization, it is a relatively complex instrument in the earliest phase of engineering evolution and has a limited vertical range of 0.2 to 1.0 μm.

For a full evaluation of the different three-dimensional PALM approaches for a particular experiment, one needs to consider the practical constraints on the sample, such as tolerable thickness range, lateral size, timescale, labeling attributes, and technical effort, along with required resolution. Resolution is not just an instrumental number, but it is, in itself, critically intertwined with the labeling approach. For example, brighter labels with more photons give better localization accuracy but are tempered by considerations such as antibody linkage length, specificity, and density of molecular labeling, whereas endogenous FP labels such as Eos have reduced brightness and require a more efficient localization use of fewer photons. Figure 4 shows this trade-off for iPALM and the defocusing techniques as a comparison of different approaches.

Dynamic, high-density molecular localization—Because of the iterative process of activation, imaging, and photobleaching, creating a single superresolution image has temporal constraints. This process can be expediated by increasing both activation and excitation light intensities to hasten the turnover of molecules, with careful attention to the health of cells. Several examples are available of live-cell imaging with photoactivatable markers to create either sequences of superresolution images (14), average distributions of or distances between molecules in living cells (15, 16), and dynamic molecular maps (17). As with any of the methods discussed above, the imaged molecular density in any single frame must remain low enough to isolate single molecules. However, the density of the localized molecules must be high enough to create a superresolution image if the aim is to measure the motions and rearrangements of protein-enriched structures on the subdiffraction-limited scale (14). For this reason, slow-moving macromolecular structures, such as adhesion complexes during cell migration (14) or endoplasmic-reticulum morphological changes (47), were appropriate candidates for proof of principle. Time series containing 25–40-s collection intervals were required to localize up to 1000 molecules μm^{-2} $frame^{-1}$ (14). The data revealed significant spatiotemporal changes in the nanoscale organization of adhesion complexes that would have been undetectable by conventional diffraction-limited imaging. For example, different zones of an individual adhesion complex moved at variable rates, recruited or lost different overall numbers of molecules, and underwent different shape changes.

Conversely, Hess et al. (16) examined hemagglutinin molecules from influenza virus and analyzed their average separations within clusters distributed across the plasma membrane. Biteen et al. (15) similarly mapped protein organization in living bacteria by imaging the bacterial actin protein MreB tagged with YFP in *Caulobacter crescentus* cells.

Manley et al. (17) tracked thousands of individual molecules in a method termed single-particle-tracking PALM (Figure 5). They then used these trajectories to compare the distribution and dynamics of two photoactivated-FP-tagged viral proteins expressed in the plasma membrane, the ts045 vesicular stomatitis viral G protein (VSVG) and the human immunodeficiency virus type 1 (HIV-1) structural protein Gag. These studies resulted in spatially resolved maps of single-molecule diffusion coefficients of these proteins, revealing strikingly different diffusional behavior: Whereas VSVG molecules were highly mobile and freely explored the plasma membrane, Gag proteins were often in immobile clusters approximating the size of viral-like particles (~100–200-nm diameter). In similar experiments in bacteria using the photoactivated FP Dendra2, the bacteria homolog of tubulin, Ftz, which forms a helical filamentous structure (i.e., Z-ring) important for bacterial cytokinesis (80), was imaged in *E. coli* to reveal both stationary and mobile molecules.

Whereas superresolution movies capture slow dynamics and rearrangements of structures, molecular tracking with photoactivation can reveal more rapid dynamics of ensembles of

molecules. Thus, these complementary methods offer molecular-scale information for biological problems with a range of different relevant timescales.

Conclusion

Superresolution imaging methods developed over the past three to four years have received increasing attention among biologists interested in understanding cellular processes at the nanoscale. Several methodologies are now available for imaging beyond the barrier imposed by diffraction. The promising illumination-based methods of STED and SSIM have pushed resolutions into the 50–100-nm range. Proponents of these approaches have rightly pointed out that STED and SSIM utilize conventional fluorophores, whereas single-molecule localization techniques such as PALM/STORM have the drawback of requiring special photoactivatable-type probes. Conventional probes have been used in single-molecule localization by relying on transitions of molecules between light and dark states, but these probably come with the loss of molecules during pre-experiment irradiation steps to lower the fluorescence to single-molecule imaging levels.

Given the commercial availability of subdiffraction-limited methods, such as STED and SSIM, why does subpixel localization of single fluorescent molecules in a dense population (i.e., PALM/STORM) generate excitement? First, the approach is fairly straightforward, and the concepts behind the techniques can be readily explained to investigators lacking training in microscopy techniques. Second, the instrumentation necessary for imaging single molecules is accessible. Third, the resolution of single-molecule localization techniques can surpass those of STED or SSIM, depending on the fluorophore and density of the molecule of interest in the specimen. Finally, single-molecule localization techniques allow the distribution and dynamics of individual molecules to be characterized relative to each other and to different molecules. This opens the possibility of examining biological questions that cannot be addressed simply by having higher resolution. Such questions include those requiring the determination of the stoichiometric arrangement of molecules within a subcellular structure and those needing the analysis of dynamic molecule motion within a subcellular environment, such as in the plasma membrane or within actin filaments, for clarifying how the molecules interact with their surroundings or participate within a molecular machine.

The future of PALM/STORM and other single-molecule localization methods is encouraging, but researchers must be mindful that these techniques began in earnest only three to four years ago, and the approaches can be considered still in the development stage. Probes need improvement, mainly in understanding or controlling their photophysical behaviors. Improvements in instrumentation and analysis could enhance the speed of the experiments and significantly decrease acquisition times. But these are growing pains that every new technique must overcome, and the ingenuity displayed thus far gives confidence that imaging below the diffraction barrier will in the next several years become as commonplace as conventional imaging today.

Acknowledgments

We thank Harald Hess (Janelia Farm Research Institute) for critical editing of this manuscript and providing Figures 3 and 4.

Literature Cited

1. Lippincott-Schwartz J, Roberts TH, Hirschberg K. Secretory protein trafficking and organelle dynamics in living cells. Annu Rev Cell Dev Biol. 2000; 16:557–89. [PubMed: 11031247]

2. Kiehart DP, Galbraith CG, Edwards KA, Rickoll WL, Montague RA. Multiple forces contribute to cell sheet morphogenesis for dorsal closure in *Drosophila*. J Cell Biol. 2000; 149:471–90. [PubMed: 10769037]
3. Kan Z, Liu TJ. Video microscopy of tumor metastasis: using the green fluorescent protein (GFP) gene as a cancer-cell-labeling system. Clin Exp Metastasis. 1999; 17:49–55. [PubMed: 10390147]
4. Tsien RY. The green fluorescent protein. Annu Rev Biochem. 1998; 67:509–44. [PubMed: 9759496]
5. Hell SW. Microscopy and its focal switch. Nat Methods. 2009; 6:24–32. [PubMed: 19116611]
6. Hell SW, Wichmann J. Breaking the diffraction resolution limit by stimulated emission: stimulated emission depletion fluorescence microscopy. Opt Lett. 1994; 19:780–82. [PubMed: 19844443]
7. Gustafsson MG. Nonlinear structured-illumination microscopy: wide-field fluorescence imaging with theoretically unlimited resolution. Proc Natl Acad Sci USA. 2005; 102:13081–86. [PubMed: 16141335]
8. Schmidt R, Wurm CA, Punge A, Egner A, Jakobs S, Hell SW. Mitochondrial cristae revealed with focused light. Nano Lett. 2009; 9:2508–10. [PubMed: 19459703]
9. Schermelleh L, Carlton PM, Haase S, Shao L, Winoto L, et al. Subdiffraction multicolor imaging of the nuclear periphery with 3D structured illumination microscopy. Science. 2008; 320:1332–36. [PubMed: 18535242]
10. Betzig E, Patterson GH, Sougrat R, Lindwasser OW, Olenych S, et al. Imaging intracellular fluorescent proteins at nanometer resolution. Science. 2006; 313:1642–45. [PubMed: 16902090]
11. Hess ST, Girirajan TP, Mason MD. Ultra-high resolution imaging by fluorescence photoactivation localization microscopy. Biophys J. 2006; 91:4258–72. [PubMed: 16980368]
12. Rust MJ, Bates M, Zhuang X. Sub-diffraction-limit imaging by stochastic optical reconstruction microscopy (STORM). Nat Methods. 2006; 3:793–95. [PubMed: 16896339]
13. Bates M, Huang B, Dempsey GT, Zhuang X. Multicolor super-resolution imaging with photoswitchable fluorescent probes. Science. 2007; 317:1749–53. [PubMed: 17702910]
14. Shroff H, Galbraith CG, Galbraith JA, Betzig E. Live-cell photoactivated localization microscopy of nanoscale adhesion dynamics. Nat Methods. 2008; 5:417–23. [PubMed: 18408726]
15. Biteen JS, Thompson MA, Tselentis NK, Bowman GR, Shapiro L, Moerner WE. Super-resolution imaging in live *Caulobacter crescentus* cells using photoswitchable EYFP. Nat Methods. 2008; 5:947–49. [PubMed: 18794860]
16. Hess ST, Gould TJ, Gudheti MV, Maas SA, Mills KD, Zimmerberg J. Dynamic clustered distribution of hemagglutinin resolved at 40 nm in living cell membranes discriminates between raft theories. Proc Natl Acad Sci USA. 2007; 104:17370–75. [PubMed: 17959773]
17. Manley S, Gillette JM, Patterson GH, Shroff H, Hess HF, et al. High-density mapping of single-molecule trajectories with photoactivated localization microscopy. Nat Methods. 2008; 5:155–57. [PubMed: 18193054]
18. Moerner WE, Kador L. Optical detection and spectroscopy of single molecules in a solid. Phys Rev Lett. 1989; 62:2535–38. [PubMed: 10040013]
19. Betzig E, Chichester RJ. Single molecules observed by near-field scanning optical microscopy. Science. 1993; 262:1422–25. [PubMed: 17736823]
20. Thompson RE, Larson DR, Webb WW. Precise nanometer localization analysis for individual fluorescent probes. Biophys J. 2002; 82:2775–83. [PubMed: 11964263]
21. Yildiz A, Forkey JN, McKinney SA, Ha T, Goldman YE, Selvin PR. Myosin V walks hand-overhand: single fluorophore imaging with 1.5-nm localization. Science. 2003; 300:2061–65. [PubMed: 12791999]
22. Yildiz A, Tomishige M, Vale RD, Selvin PR. Kinesin walks hand-overhand. Science. 2004; 303:676–78. [PubMed: 14684828]
23. Hess HF, Betzig E, Harris TD, Pfeiffer LN, West KW. Near-field spectroscopy of the quantum constituents of a luminescent system. Science. 1994; 264:1740–45. [PubMed: 17839907]
24. Betzig E. Proposed method for molecular optical imaging. Opt Lett. 1995; 20:237–39. [PubMed: 19859146]

25. Patterson GH, Lippincott-Schwartz J. A photoactivatable GFP for selective photolabeling of proteins and cells. Science. 2002; 297:1873–77. [PubMed: 12228718]
26. Lippincott-Schwartz J, Patterson GH. Photoactivatable fluorescent proteins for diffraction-limited and super-resolution imaging. Trends Cell Biol. 2009; 19:555–65. [PubMed: 19836954]
27. Fernandez-Suarez M, Ting AY. Fluorescent probes for super-resolution imaging in living cells. Nat Rev Mol Cell Biol. 2008; 9:929–43. [PubMed: 19002208]
28. Heilemann M, van de Linde S, Mukherjee A, Sauer M. Super-resolution imaging with small organic fluorophores. Angew Chem Int Ed Engl. 2009; 48:6903–8. [PubMed: 19670280]
29. Huang B, Bates M, Zhuang X. Super-resolution fluorescence microscopy. Annu Rev Biochem. 2009; 78:993–1016. [PubMed: 19489737]
30. McKinney SA, Murphy CS, Hazelwood KL, Davidson MW, Looger LL. A bright and photostable photoconvertible fluorescent protein. Nat Methods. 2009; 6:131–33. [PubMed: 19169260]
31. Shroff H, Galbraith CG, Galbraith JA, White H, Gillette J, et al. Dual-color superresolution imaging of genetically expressed probes within individual adhesion complexes. Proc Natl Acad Sci USA. 2007; 104:20308–13. [PubMed: 18077327]
32. Day RN, Davidson MW. The fluorescent protein palette: tools for cellular imaging. Chem Soc Rev. 2009; 38:2887–921. [PubMed: 19771335]
33. Cubitt, AB.; Woollenweber, LA.; Heim, R. Understanding structure-function relationships in the *Aequorea victoria* green fluorescent protein. In: Sullivan, KF.; Kay, SA., editors. Green Fluorescent Proteins. San Diego: Academic; 1997. p. 19-30.
34. Dickson RM, Cubitt AB, Tsien RY, Moerner WE. On/off blinking and switching behavior of single molecules of green fluorescent protein. Nature. 1997; 388:355–58. [PubMed: 9237752]
35. Shaner NC, Patterson GH, Davidson MW. Advances in fluorescent protein technology. J Cell Sci. 2007; 120:4247–60. [PubMed: 18057027]
36. Subach FV, Patterson GH, Manley S, Gillette JM, Lippincott-Schwartz J, Verkhusha VV. Photoactivatable mCherry for high-resolution two-color fluorescence microscopy. Nat Methods. 2009; 6:153–59. [PubMed: 19169259]
37. Chudakov DM, Verkhusha VV, Staroverov DB, Souslova EA, Lukyanov S, Lukyanov KA. Photoswitchable cyan fluorescent protein for protein tracking. Nat Biotechnol. 2004; 22:1435–39. [PubMed: 15502815]
38. Matsuda T, Miyawaki A, Nagai T. Direct measurement of protein dynamics inside cells using a rationally designed photoconvertible protein. Nat Methods. 2008; 5:339–45. [PubMed: 18345008]
39. Wiedenmann J, Ivanchenko S, Oswald F, Schmitt F, Rocker C, et al. EosFP, a fluorescent marker protein with UV-inducible green-to-red fluorescence conversion. Proc Natl Acad Sci USA. 2004; 101:15905–10. [PubMed: 15505211]
40. Nienhaus GU, Nienhaus K, Holzle A, Ivanchenko S, Renzi F, et al. Photoconvertible fluorescent protein EosFP: biophysical properties and cell biology applications. Photochem Photobiol. 2006; 82:351–58. [PubMed: 16613485]
41. Habuchi S, Tsutsui H, Kochaniak AB, Miyawaki A, van Oijen AM. mKikGR, a monomeric photoswitchable fluorescent protein. PLoS One. 2008; 3:e3944. [PubMed: 19079591]
42. Gurskaya NG, Verkhusha VV, Shcheglov AS, Staroverov DB, Chepurnykh TV, et al. Engineering of a monomeric green-to-red photoactivatable fluorescent protein induced by blue light. Nat Biotechnol. 2006; 24:461–65. [PubMed: 16550175]
43. Adam V, Lelimousin M, Boehme S, Desfonds G, Nienhaus K, et al. Structural characterization of IrisFP, an optical highlighter undergoing multiple photo-induced transformations. Proc Natl Acad Sci USA. 2008; 105:18343–48. [PubMed: 19017808]
44. Kremers GJ, Hazelwood KL, Murphy CS, Davidson MW, Piston DW. Photoconversion in orange and red fluorescent proteins. Nat Methods. 2009; 6:355–58. [PubMed: 19363494]
45. Ando R, Mizuno H, Miyawaki A. Regulated fast nucleocytoplasmic shuttling observed by reversible protein highlighting. Science. 2004; 306:1370–73. [PubMed: 15550670]
46. Habuchi S, Ando R, Dedecker P, Verheijen W, Mizuno H, et al. Reversible single-molecule photoswitching in the GFP-like fluorescent protein Dronpa. Proc Natl Acad Sci USA. 2005; 102:9511–16. [PubMed: 15972810]

47. Andresen M, Stiel AC, Folling J, Wenzel D, Schonle A, et al. Photoswitchable fluorescent proteins enable monochromatic multilabel imaging and dual color fluorescence nanoscopy. Nat Biotechnol. 2008; 26:1035–40. [PubMed: 18724362]
48. Stiel AC, Trowitzsch S, Weber G, Andresen M, Eggeling C, et al. 1.8 A bright-state structure of the reversibly switchable fluorescent protein Dronpa guides the generation of fast switching variants. Biochem J. 2007; 402:35–42. [PubMed: 17117927]
49. Chudakov DM, Belousov VV, Zaraisky AG, Novoselov VV, Staroverov DB, et al. Kindling fluorescent proteins for precise in vivo photolabeling. Nat Biotechnol. 2003; 21:191–94. [PubMed: 12524551]
50. Henderson JN, Ai HW, Campbell RE, Remington SJ. Structural basis for reversible photobleaching of a green fluorescent protein homologue. Proc Natl Acad Sci USA. 2007; 104:6672–77. [PubMed: 17420458]
51. Stiel AC, Andresen M, Bock H, Hilbert M, Schilde J, et al. Generation of monomeric reversibly switchable red fluorescent proteins for far-field fluorescence nanoscopy. Biophys J. 2008; 95:2989–97. [PubMed: 18658221]
52. Politz JC. Use of caged fluorophores to track macromolecular movement in living cells. Trends Cell Biol. 1999; 9:284–87. [PubMed: 10370245]
53. Bates M, Blosser TR, Zhuang X. Short-range spectroscopic ruler based on a single-molecule optical switch. Phys Rev Lett. 2005; 94:108101. [PubMed: 15783528]
54. Michalet X, Pinaud FF, Bentolila LA, Tsay JM, Doose S, et al. Quantum dots for live cells, in vivo imaging, and diagnostics. Science. 2005; 307:538–44. [PubMed: 15681376]
55. Irvine SE, Staudt T, Rittweger E, Engelhardt J, Hell SW. Direct light-driven modulation of luminescence from Mn-doped ZnSe quantum dots. Angew Chem Int Ed Engl. 2008; 47:2685–88. [PubMed: 18306194]
56. Lavis LD, Raines RT. Bright ideas for chemical biology. ACS Chem Biol. 2008; 3:142–55. [PubMed: 18355003]
57. Folling J, Belov V, Kunetsky R, Medda R, Schonle A, et al. Photochromic rhodamines provide nanoscopy with optical sectioning. Angew Chem Int Ed Engl. 2007; 46:6266–70. [PubMed: 17640007]
58. Bates M, Huang B, Zhuang X. Super-resolution microscopy by nanoscale localization of photoswitchable fluorescent probes. Curr Opin Chem Biol. 2008; 12:505–14. [PubMed: 18809508]
59. Donnert G, Eggeling C, Hell SW. Major signal increase in fluorescence microscopy through dark-state relaxation. Nat Methods. 2007; 4:81–86. [PubMed: 17179937]
60. Heilemann M, Margeat E, Kasper R, SauerM, Tinnefeld P. Carbocyanine dyes as efficient reversible single-molecule optical switch. J Am Chem Soc. 2005; 127:3801–6. [PubMed: 15771514]
61. Chen I, Ting AY. Site-specific labeling of proteins with small molecules in live cells. Curr Opin Biotechnol. 2005; 16:35–40. [PubMed: 15722013]
62. Lin MZ, Wang L. Selective labeling of proteins with chemical probes in living cells. Physiology (Bethesda). 2008; 23:131–41. [PubMed: 18556466]
63. Adams SR, Campbell RE, Gross LA, Martin BR, Walkup GK, et al. New biarsenical ligands and tetracysteine motifs for protein labeling in vitro and in vivo: synthesis and biological applications. J Am Chem Soc. 2002; 124:6063–76. [PubMed: 12022841]
64. van Oijen AM, Kühler J, Schmidt J, Müller M, Brakenhoff GJ. Three-dimensional super-resolution by spectrally selective imaging. Chem Phys Lett. 1998; 292:183–87.
65. van Oijen AM, Kühler J, Schmidt J, Müller M, Brakenhoff GJ. Far-field fluorescence microscopy beyond the diffraction limit. J Opt Soc Am. 1999; 16:909–15.
66. Heilemann M, Herten DP, Heintzmann R, Cremer C, Muller C, et al. High-resolution colocalization of single dye molecules by fluorescence lifetime imaging microscopy. Anal Chem. 2002; 74:3511–17. [PubMed: 12139062]
67. Qu X, Wu D, Mets L, Scherer NF. Nanometer-localized multiple single-molecule fluorescence microscopy. Proc Natl Acad Sci USA. 2004; 101:11298–303. [PubMed: 15277661]

68. Lidke KA, Rieger B, Jovin TM, Heintzmann R. Superresolution by localization of quantum dots using blinking statistics. Opt Expr. 2005; 13:7052–62.
69. Geisler C, Schonle A, Von Middendorff C, Bock H, Eggeling C, et al. Resolution of λ/10 in fluorescence microscopy using fast single molecule photo-switching. Appl Phys A. 2007; 88:223–26.
70. Heilemann M, van de Linde S, Schuttpelz M, Kasper R, Seefeldt B, et al. Subdiffraction-resolution fluorescence imaging with conventional fluorescent probes. Angew Chem Int Ed Engl. 2008; 47:6172–76. [PubMed: 18646237]
71. Baddeley D, Jayasinghe ID, Cremer C, Cannell MB, Soeller C. Light-induced dark states of organic fluochromes enable 30 nm resolution imaging in standard media. Biophys J. 2009; 96:L22–24. [PubMed: 19167284]
72. Folling J, Bossi M, Bock H, Medda R, Wurm CA, et al. Fluorescence nanoscopy by ground-state depletion and single-molecule return. Nat Methods. 2008; 5:943–45. [PubMed: 18794861]
73. Pavani SR, Thompson MA, Biteen JS, Lord SJ, Liu N, et al. Three-dimensional, single-molecule fluorescence imaging beyond the diffraction limit by using a double-helix point spread function. Proc Natl Acad Sci USA. 2009; 106:2995–99. [PubMed: 19211795]
74. Greenfield D, McEvoy AL, Shroff H, Crooks GE, Wingreen NS, et al. Self-organization of the *Escherichia coli* chemotaxis network imaged with super-resolution light microscopy. PLoS Biol. 2009; 7:e1000137. [PubMed: 19547746]
75. Bock H, Geisler C, Wurm CA, von Middendorff C, Jakobs S, et al. Two-color far-field fluorescence nanoscopy based on photoswitchable emitters. Appl Phys B. 2007; 88:161–65.
76. Juette MF, Gould TJ, Lessard MD, Mlodzianoski MJ, Nagpure BS, et al. Three-dimensional sub-100 nm resolution fluorescence microscopy of thick samples. Nat Methods. 2008; 5:527–29. [PubMed: 18469823]
77. Huang B, Wang W, Bates M, Zhuang X. Three-dimensional super-resolution imaging by stochastic optical reconstruction microscopy. Science. 2008; 319:810–13. [PubMed: 18174397]
78. Vaziri A, Tang J, Shroff H, Shank CV. Multilayer three-dimensional super resolution imaging of thick biological samples. Proc Natl Acad Sci USA. 2008; 105:20221–26. [PubMed: 19088193]
79. Shtengel G, Galbraith JA, Galbraith CG, Lippincott-Schwartz J, Gillette JM, et al. Interferometric fluorescent super-resolution microscopy resolves 3D cellular ultrastructure. Proc Natl Acad Sci USA. 2009; 106:3125–30. [PubMed: 19202073]
80. Niu L, Yu J. Investigating intracellular dynamics of FtsZ cytoskeleton with photoactivation single-molecule tracking. Biophys J. 2008; 95:2009–16. [PubMed: 18390602]
81. Ando R, Hama H, Yamamoto-Hino M, Mizuno H, Miyawaki A. An optical marker based on the UV-induced green-to-red photoconversion of a fluorescent protein. Proc Natl Acad Sci USA. 2002; 99:12651–56. [PubMed: 12271129]
82. Flors C, Hotta J, Uji-i H, Dedecker P, Ando R, et al. A stroboscopic approach for fast photoactivation-localization microscopy with Dronpa mutants. J Am Chem Soc. 2007; 129:13970–77. [PubMed: 17956094]
83. Bizzarri R, Arcangeli C, Arosio D, Ricci F, Faraci P, et al. Development of a novel GFP-based ratiometric excitation and emission pH indicator for intracellular studies. Biophys J. 2006; 90:3300–14. [PubMed: 16603505]

Glossary

FP	fluorescent protein
Superresolution	resolution that is greater than the diffraction limit of light through a lens (i.e., better than 200 nm along the *x*–*y* axis and 500 nm along the *z* axis)
Illumination-based superresolution imaging	imaging using nonlinear optical approaches to reduce the focal spot size as in STED and SSIM

STED	stimulated emission depletion fluorescence microscopy
SSIM	saturated structured illumination microscopy
Probe-based superresolution imaging	imaging using photoswitchable molecules to resolve dense populations of molecules by temporally switching on one molecule at a time in the population, determining its single-molecule position, and then summing together all molecular positions for a superresolution image as in PALM, FPALM, and STORM
PALM	photoactivated localization microscopy
FPALM	fluorescence photoactivated localization microscopy
Photoactivatable fluorescent protein	a fluorescent protein that switches from a dark state to a bright state in response to ultraviolet light
Photoconvertible fluorescent protein	a fluorescent protein that undergoes photoconversion from one emission wavelength to another, usually from green to red, in response to ultraviolet light
STORM	stochastic optical reconstruction microscopy
Diffraction limit	limit in resolving capability of conventional light microscopy
Quantum dot	inorganic semiconductor nanocrystal that exhibits bright fluorescence over a large wavelength range
Optical highlighter	fluorescent protein that switches on fluorescence from a dark or different fluorescent state using photoactivation, photoconversion, or photoswitching techniques
Point spread function (PSF)	diffraction-limited blurred spot obtained when a single point source light emitter is focused through a lens
Nyquist criterion	states that the minimal sampling density needed to capture information from an image is two data points per resolution unit

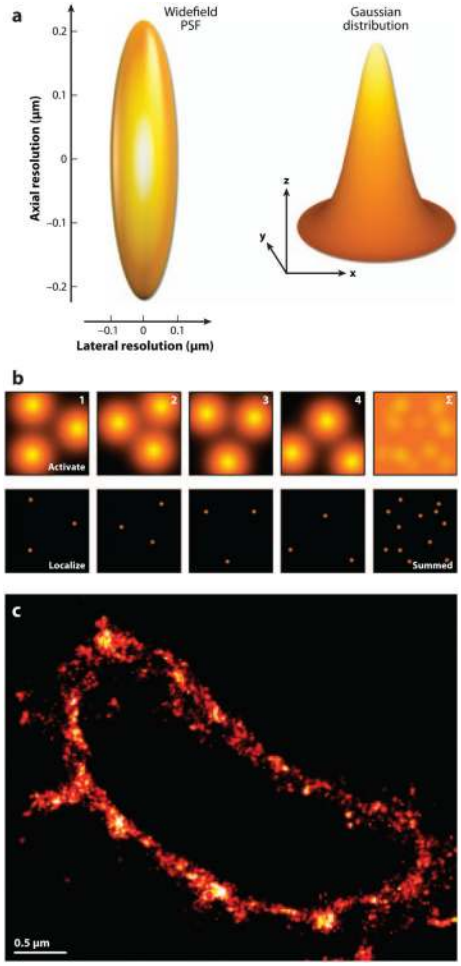

Figure 1.

The point spread function (PSF) and principle of single-molecule superresolution imaging. (*a*) Focused light through a lens always produces a blurred or diffracted spot that is commonly represented by the PSF (*left panel*) with dimensions of ~200 nm laterally (*x*, *y*) and ~500 nm axially (*z*) for green light imaged through a lens having a numerical aperture of 1.4. The lateral PSF of a fluorescent point emitter can be fitted to a two-dimensional Gaussian distribution (*right panel*) to obtain the centroid of the fluorescent probe with nanometric accuracy. This is a key principle of single-molecule superresolution: fitting with high precision the centroid of a diffracted, blurry spot from a fluorescent molecule. (*b*) Single-molecule superresolution in practice is achieved by illuminating a densely populated specimen with low-intensity activation light so that only a sparse pool of molecules is activated. The position of each molecule is localized by fitting the measured photon distribution with a two-dimensional Gaussian function. These molecules are then photobleached before additional cycles of activation and photobleaching of new molecules are performed. A composite superresolution image (see the panel marked “Summed”) that contains information about the localization of many single molecules can thereby be produced within a single diffraction-limited region. (*c*) PALM image of a thin section through a lysosome expressing CD63 tagged with the photoactivated fluorescent protein Kaede, revealing highly localized molecules on the membranes of this organelle. Figure adapted from Reference 10.

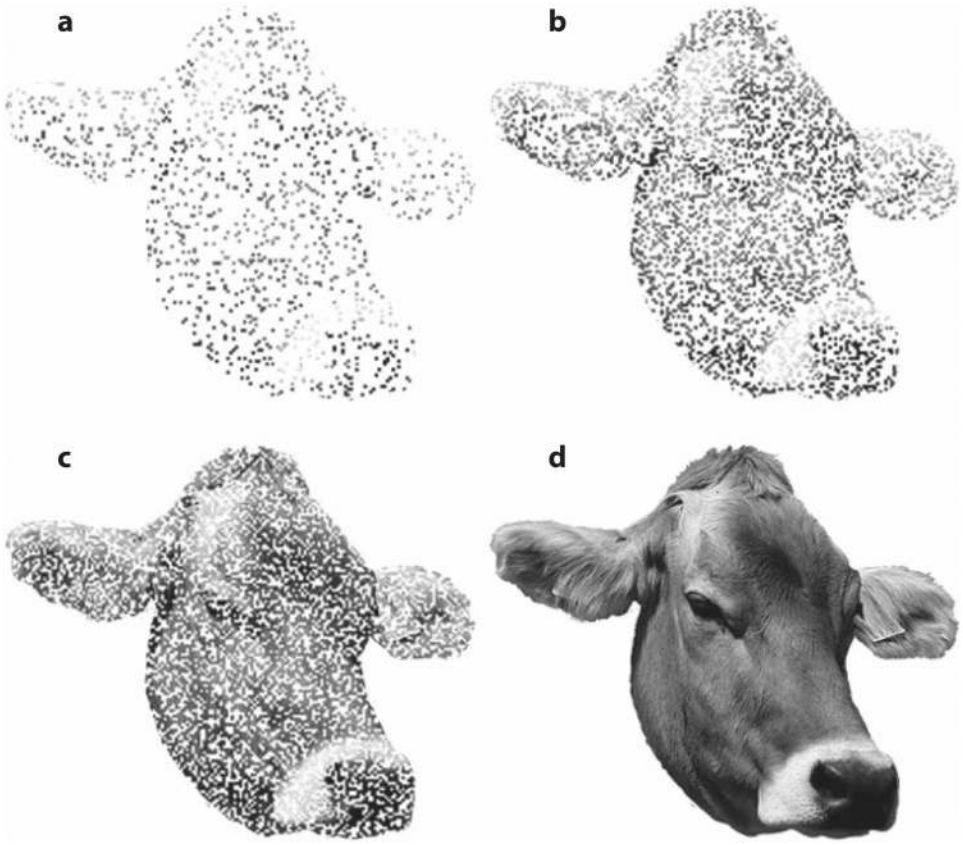

Figure 2.
Localization precision, resolution, and molecular density in single-molecule localization techniques. This series of images of Bossy the cow demonstrates how the superresolution image is built by plotting localized molecules, depicted here as points. For the purposes of illustration, the point sizes in panels *a*–*c* are depicted much larger than would be necessary to achieve the final image shown in panel *d*. The image of Bossy in panel *a* shows many localized points, but the relatively low density does not allow recognition of the image. As more points are placed in the images in panels *b* and *c*, it becomes more recognizable, but distinguishing (resolving) the fine features associated with Bossy's image requires a higher density of points, as shown in panel *d*. Thus, an image can be produced that contains precisely localized points using single-molecule localization techniques, but the density of those points affects directly the capability to resolve the features of the image.

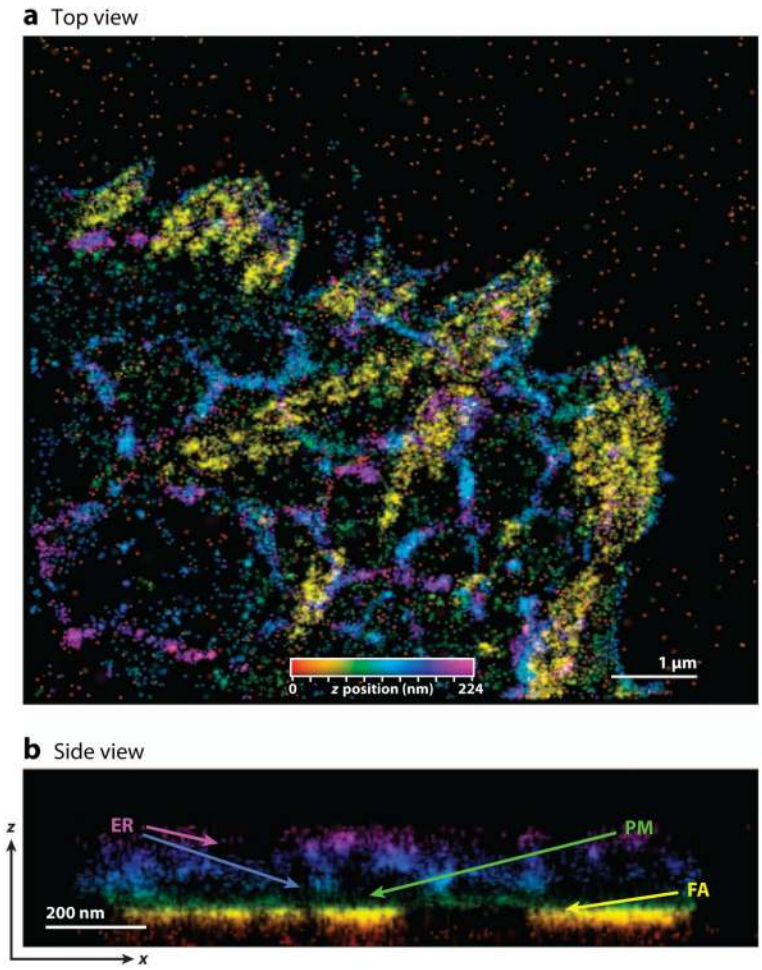

Figure 3.

iPALM image showing the three-dimensional localization of αv-integrin tagged with td-EosFP in a U2OS cell. Single molecules are color-coded based on their *z* position (see the color scale in the panel *a*), with red molecules closest to the coverslip, followed by yellow, blue, and purple molecules at further distances. Displayed in both the top and side views, integrin molecules distribute at multiple cellular sites. In addition to their concentration within feet-like focal adhesions (FA) found near the coverslip (see the *yellow molecules*), they can be seen in the plasma membrane (PM, *green molecules*) and in the tubular network comprising the endoplasmic reticulum (ER, *blue-purple molecules*) positioned ~100–200 nm up from the PM. Figure adapted from Reference 79.

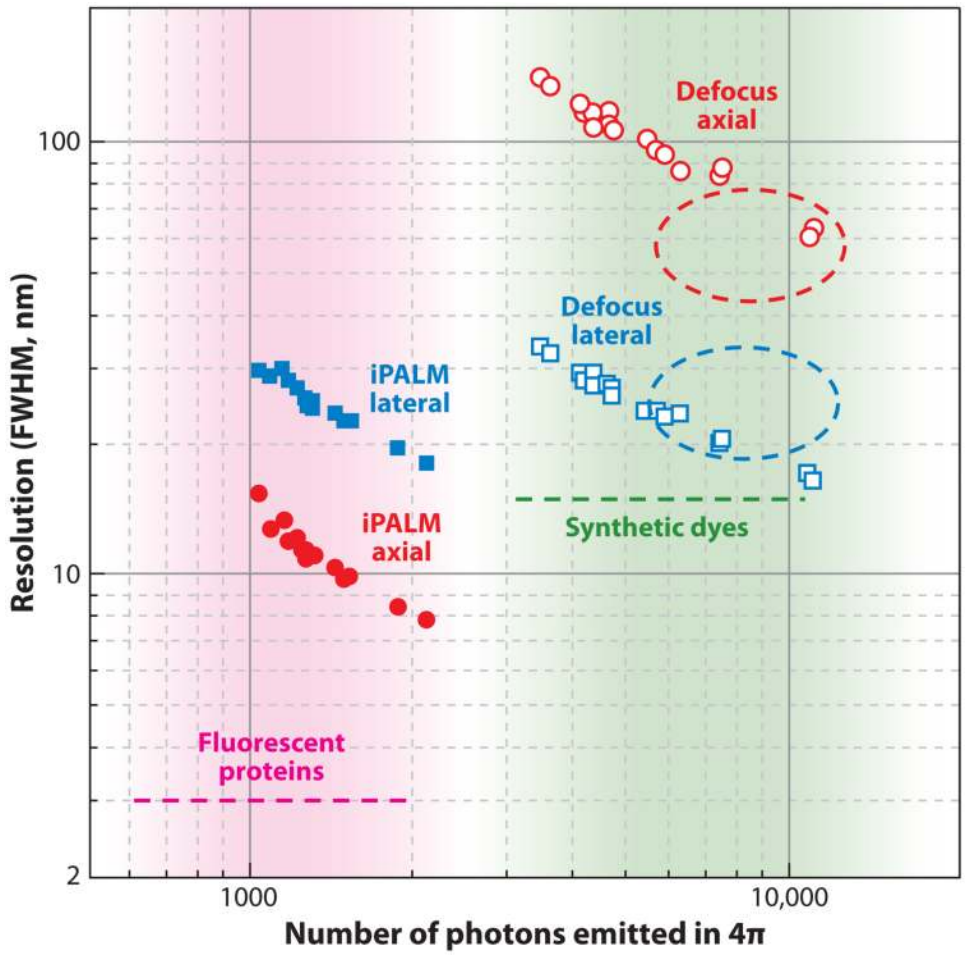

Figure 4.

Comparison of three-dimensional single-molecule localization techniques. The three-dimensional precision of iPALM and defocusing techniques is shown as a function of the number of photons emitted from gold beads. iPALM (*filled circles and filled squares*) has better localization precision per emitted photon than defocusing techniques (*unfilled circles and squares*) and displays better axial (*filled red circles*) than lateral (*filled blue squares*) resolution. Conversely, defocusing techniques have markedly less precision per emitted photon in the axial direction (*unfilled red circles*) compared with the lateral direction (*unfilled blue squares*). FWHM, full width at half-maximum. Figure redrawn from Reference 79.

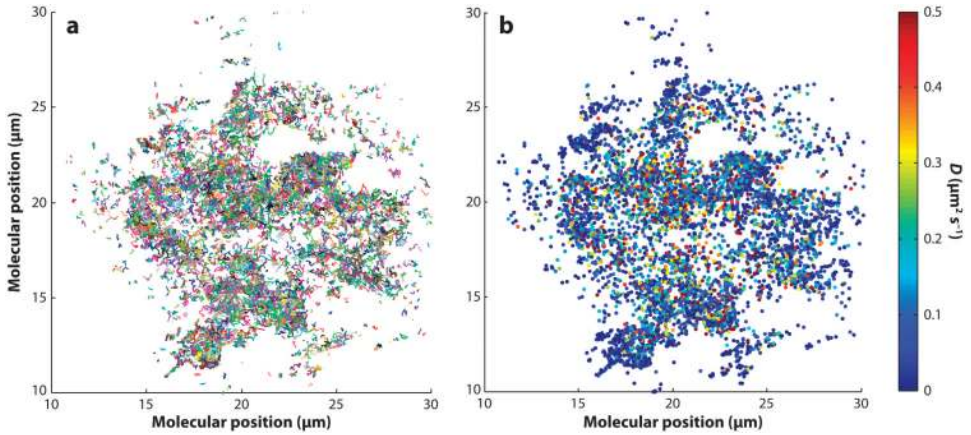

Figure 5.

Imaging dynamic, dense populations using single-particle-tracking PALM. The molecular motion of VSVG-tdEosFP was imaged in a COS 7 cell using 561-nm light while simultaneously photoactivating subsets of the tdEosFP molecules. (*a*) The molecules were localized in each frame, and their determined positions in consecutive frames were linked into tracks. These represent molecules that fluoresced for > 0.75 s and are plotted as different colors to distinguish individual tracks. (*b*) The diffusion coefficient for each track was determined and plotted as a filled circle at the start of the track. Each has been assigned a color based on its value of D (see color scale on right).

Table 1

Properties of selected optical highlighter fluorescent protein derivatives

Protein (acronym)	Ex[a] (nm)	Em (nm)	EC ($\times 10^{-3}$ $M^{-1}cm^{-1}$)	QY	Quaternary structure	Relative brightness[b] (% of EGFP)	Reference
Photoactivatable fluorescent proteins							
PA-GFP (N)	400	515	20.7	0.13	Monomer	8	25
PA-GFP (G)	504	517	17.4	0.79	Monomer	41	25
PS-CFP2 (C)	400	468	43.0	0.20	Monomer	26	37
PS-CFP2 (G)	490	511	47.0	0.23	Monomer	32	37
PA-mCherry1 (R)	564	595	18.0	0.46	Monomer	25	36
Phamret (C)	458	475	32.5	0.40	Monomer	39	38
Phamret (G)	458	517	17.4	0.79	Monomer	41	38
Photoconvertible fluorescent proteins							
mKikGR (G)	505	515	49.0	0.69	Monomer	101	41
mKikGR (R)	580	591	28.0	0.63	Monomer	53	41
tdEos (G)	506	516	84.0	0.66	Tandem dimer	165	40
tdEos (R)	569	581	33.0	0.60	Tandem dimer	59	40
mEos2 (G)	506	519	56.0	0.84	Monomer	140	30
mEos2 (R)	573	584	46.0	0.66	Monomer	90	30
Dendra2 (G)	490	507	45.0	0.50	Monomer	67	42
Dendra2 (R)	553	573	35.0	0.55	Monomer	57	42
Photoswitchable fluorescent proteins							
Dronpa	503	517	95.0	0.85	Monomer	240	81
Dronpa-3	487	514	58.0	0.33	Monomer	56	82
rsFastLine	496	518	39.1	0.77	Monomer	89	48
Padron	503	522	43.0	0.64	Monomer	82	47
bsDronpa	460	504	45.0	0.50	Monomer	67	47
KFP1	580	600	59.0	0.07	Tetramer	12	49
mTFP0.7	453	488	60.0	0.50	Monomer	89	50
E2GFP	515	523	29.3	0.91	Monomer	79	83
rsCherry	572	610	80.0	0.02	Monomer	5	51

Protein (acronym)	Ex[a] (nm)	Em (nm)	EC ($\times 10^{-3}$ $M^{-1}cm^{-1}$)	QY	Quaternary structure	Relative brightness[b] (% of EGFP)	Reference
rsCherryRev	572	608	84.0	0.005	Monomer	1	51
Photoconvertible/photoswitchable fluorescent proteins							
IrisFP (G)	488	516	52.2	0.43	Tetramer	67	43
IrisFP (R)	551	580	35.4	0.47	Tetramer	50	43

[a] Abbreviations: Ex, excitation wavelength; Em, emission wavelength; EC, molar extinction coefficient; QY, quantum yield.

[b] The computed brightness values were derived from the product of the molar extinction coefficient and quantum yield, divided by the value for EGFP.